Chemical Science

ROYAL SOCIETY OF CHEMISTRY

EDGE ARTICLE

View Article Online
View Journal | View Issue

Check for updates

Cite this: *Chem. Sci.*, 2024, **15**, 9318

All publication charges for this article have been paid for by the Royal Society of Chemistry

Received 22nd April 2024
Accepted 10th May 2024

DOI: 10.1039/d4sc02659d

rsc.li/chemical-science

Systemic regulation of binding sites in porous coordination polymers for ethylene purification from ternary C2 hydrocarbons†

Yi Li,[a] Yanxin Wu,[a] Jiaxin Zhao,[a] Jingui Duan *[ab] and Wanqin Jin *[a]

The global demand for poly-grade ethylene (C_2H_4) is increasing annually. However, the energy-saving purification of this gas remains a major challenge due to the similarity in molecular properties among the ternary C2 hydrocarbons. To address this challenge, we report an approach of systematic tuning of the pore environment with organic sites (from –COOH to $-CF_3$, then to $-CH_3$) in porous coordination polymers (PCPs), of which **NTU-73-CH$_3$** shows remarkable capability for the direct production of poly-grade C_2H_4 from ternary C2 hydrocarbons under ambient conditions. In comparison, the precursor structure of **NTU-73-COOH** is unable to purify C_2H_4, while **NTU-73-CF$_3$** shows minimal ability to harvest C_2H_4. This is because the changed binding sites in the **NTU-73-series** not only eliminate the channel obstruction caused by the formation of gas clusters, but also enhance the interaction with acetylene (C_2H_2) and ethane (C_2H_6), as validated by *in situ* crystallographic and Raman analysis. Our findings, in particular the systematic tuning of the pore environment and the efficient C_2H_4 purification by **NTU-73-CH$_3$**, provide a blueprint for the creation of advanced porous families that can handle desired tasks.

Introduction

Ethylene (C_2H_4) is used as an important building block in industry for the production of value-added organics.[1–3] Currently, C_2H_4 is mainly obtained by separating the downstream of cracking of naphtha, C2 hydrocarbon gas mixtures during the steam cracking process.[4–6] Typically, acetylene (C_2H_2) is removed by solvent extraction or catalytic hydrogenation, which requires large equipment, as well as large amounts of solvents or higher temperature.[7,8] Subsequently, ethane (C_2H_6) is removed through cryogenic distillation, a type of huge energy-consuming process.[9]

The energy-intensive and cost-effective processes have spurred research into the development of energy-efficient approaches.[10] Adsorptive separation, with a significant character of energy efficiency, has been considered as a kind of alternative or transition technology.[11] Porous coordination polymers (PCPs),[12–16] covalent organic frameworks (COFs),[17,18] zeolites,[19–21] and carbon materials[22] have been explored for gas separation. Thanks to the rational pore tuning and straightforward pore functionalization, PCPs have shown good performance as adsorbents for various gas separations, but only a few examples can purify C_2H_4 from binary mixtures containing C_2H_2 or C_2H_6. However, from an energy point of view, it is crucial to remove both by-products in one-step with an adsorbent, but the challenge is enormous.[23–25]

In general, the preferential adsorption of C_2H_2 over C_2H_4 requires the pore to contain highly polar sites (such as inorganic anionic pillars and open metal sites) due to the larger quadrupole moment (7.2×10^{-26} *vs.* 1.5×10^{-26} esu cm^2) and higher acidity (pK_a: 45 *vs.* 26) of C_2H_2, resulting in strong host–C_2H_2 electrostatic interactions.[26] Conversely, the greater polarizability of C_2H_6 (44.7×10^{-25} *vs.* 42.5×10^{-25} cm^3) contributes to the relatively weak van der Waals interactions with the structural framework modified low polarity sites.[27–30] To address this conflict, very few studies have been reported, primarily by exploiting the supramolecular interactions. The early framework of TJT-100 demonstrates the simultaneous capture of C_2H_2 and C_2H_6 through a hierarchy of interactions between the electronegative carboxylate O atoms and the gases.[11] A similar interaction has also been observed in NPU-1.[31] By incorporating the $-NH_2$ group or exposing the N site, UiO-67-NH_2 and Al-PyDC also show preferential adsorption of C_2H_2 and C_2H_6.[32,33] Additionally, the cyclopentadiene-cobalt functional group in the UPC-series allows for efficient separation of C2 hydrocarbon mixtures. More promisingly, the synergistic sorbent separation technology (also called Lego-brick strategy) enables the production of high-purity C_2H_4 from a quaternary mixture of

[a]*State Key Laboratory of Materials-Oriented Chemical Engineering, Nanjing Tech University, Nanjing 211816, China. E-mail: duanjingui@njtech.edu.cn; wqjin@njtech.edu.cn*

[b]*State Key Laboratory of Chemistry and Utilization of Carbon Based Energy Resources, College of Chemistry, Xinjiang University, Urumqi, 830017, China*

† Electronic supplementary information (ESI) available: Synthesis and characterization of the three crystals, PXRD, TGA, IR, sorption isotherms, IAST, breakthrough experiments and fitting parameters. CCDC 2337168–2337175. For ESI and crystallographic data in CIF or other electronic format see DOI: https://doi.org/10.1039/d4sc02659d

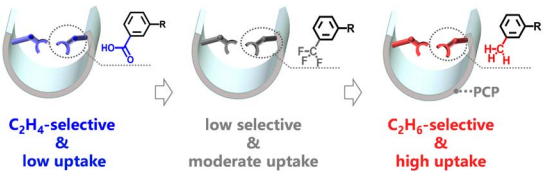

Scheme 1 Systemic tuning of the functional sites in PCPs for efficient C_2H_4 purification.

$C_2H_6/C_2H_4/C_2H_2/CO_2$ by utilizing tandem packing of carefully selected PCPs, with each PCP acting as a separator for binary mixtures.[25,34] Although these individual materials exhibit the desired functions, further systematic exploration is urgently needed due to the abundance and facile tunability of the supramolecular sites.

We are interested in the separation of light hydrocarbons using finely designed PCPs.[35–39] Recently, we have reported a new family of PCPs with crab-like carboxylic pincers, which allows for high C_2H_2/C_2H_4 selectivity and an unprecedented ability to obtain high-purity forms of both gases.[40] However, the strong binding interaction allows the absorbed C_2H_2 to form a tetrameric gas cluster at the channel neck, which strongly blocks the accessibility of the adjacent large cavity. Inspired by the unique porous nature of **NTU-73** and also by the function of supramolecular sites, we report here a systematic tuning of functional sites in this porous platform, where the carboxylic pincers on the pore wall (corresponding **L1**: 3,5-di(1*H*-imidazol-1-yl)benzoic acid) were replaced with $-CF_3$ (corresponding **L2**: 1,1′-(5-(trifluoromethyl)-1,3-phenylene)bis(1*H*-imidazole)) or $-CH_3$ (corresponding **L3**: 1,1′-(5-methyl-1,3-phenylene)bis(1*H*-imidazole)) (Scheme 1). The highly stable **NTU-73-CH$_3$** exhibits a remarkable ability to directly produce poly-grade C_2H_4 from ternary C2 hydrocarbons, while, **NTU-73-CF$_3$** and **NTU-73-COOH** can only exhibit minimal capacity or are unable to achieve C_2H_4 purification at all. These results reflect the positive effect of changing functional sites on strengthening the host–guest interactions and the stability of the framework.

Experimental section

General procedures of the experiments and simulation are available in the ESI.†

Synthesis of NTU-73-series

Synthesis of NTU-73-COOH. NTU-73-COOH was synthesized according to our previous work.[40]

Synthesis of NTU-73-CF$_3$. $Cu(BF_4)_2 \cdot 6H_2O$ (10 mg, 0.039 mmol), **L2** (5 mg, 0.018 mmol) and H_2ZrF_6 (50 μL, 45%) were mixed in *N*,*N*′-dimethylacetamide (DMA)/H_2O/ethanol (EtOH) (0.5/0.25/0.75, v/v/v, 1.5 mL) and reacted at 90 °C for 2 days to obtain blue block crystals. After cooling down, the crystals were washed three times with fresh DMA (yield: ~52%, based on **L2**).

Synthesis of NTU-73-CH$_3$. $Cu(BF_4)_2 \cdot 6H_2O$ (10 mg, 0.039 mmol), **L3** (5 mg, 0.022 mmol) and H_2ZrF_6 (50 μL, 45%) were added to the DMA/H_2O/EtOH (0.5/0.25/0.75, 1.5 mL) mixed solvent and reacted at 90 °C for 2 days to give blue block crystals. After cooling down, the crystals were washed three times with fresh DMA (yield: ~60%, based on **L3**).

Results and discussion

Crystal structures and characterization

Solvent-thermal reactions of copper(II) hexafluorozirconium with corresponding ligands yielded polyhedron-shaped crystals (**NTU-73-series**). These crystals all crystallized in a tetragonal $I4_122$ space group with the formula of $[Cu(L)_2ZrF_6]\cdot x$Guest (Table S1†). Two of our newly synthesized crystals (**NTU-73-CF$_3$** and **NTU-73-CH$_3$**) have the same coordination mode as that of **NTU-73-COOH**. The asymmetric unit of all three PCPs consists of one ligand, half a Cu^{2+} ion and half a ZrF_6^{2-} anion. Each Cu node is coordinated by two F atoms from the two ZrF_6^{2-} anions and four imidazole N atoms from four ligands (Fig. S3–S5†). Additionally, two helical chains linked by ZrF_6^{2-} anions are present in the frameworks (Fig. S6†). Differently, the carboxylic-modified channel wall observed from two different directions in **NTU-73-COOH** has been replaced by a couple of $-CF_3$ or $-CH_3$ groups in **NTU-73-CF$_3$** and **NTU-73-CH$_3$** (Fig. S7–S12†), respectively. Furthermore, there is an overall trend of increasing pore size (**NTU-73-COOH**: 4.5 × 5.2 Å^2 and 3.9 × 5.6 Å^2; **NTU-73-CF$_3$**: 3.7 × 5.2 Å^2 and 4.2 × 7.8 Å^2; **NTU-73-CH$_3$**: 4.4 × 5.4 Å^2 and 6.2 × 9.2 Å^2) as the functional group size gradually decreases (Fig. 1). Considering the unique ability of **NTU-73-COOH** to separate C_2H_2/C_2H_4 and the systematic changes in the pore environment, including binding sites and pore size, we expected this platform to be highly efficient for the C2 ternary mixture separation. The phase purity of the crystals was confirmed by powder X-ray diffraction (PXRD) as the diffraction peaks of the synthesized and activated **NTU-73-series** were in good agreement with the simulated patterns (Fig. S13–S15†).

Pore evaluation

The permanent porosity of the **NTU-73-series** was investigated through N_2 (77 K) and CO_2 (195 K) adsorption measurements (Fig. 2a and S22†). Although **NTU-73-COOH** exhibits negligible N_2 uptake, the two newly prepared PCPs show improved N_2 adsorption, with maximum uptakes of 193 and 295 cm^3 g^{-1}, respectively. Interestingly, all three PCPs show type-I and significant CO_2 adsorption isotherms. The maximum uptake increases from 63 (**NTU-73-COOH**) to 250 cm^3 g^{-1} (**NTU-73-CH$_3$**). For consistency, the Brunauer–Emmett–Teller surface areas of the **NTU-73-series** were calculated based on CO_2 isotherms. The BET surface areas of the **NTU-73-series** were calculated to be 228, 889 and 1078 m^2 g^{-1}, respectively, with corresponding pore volumes of 0.039, 0.153 and 0.185 m^3 g^{-1} (Table S2†). Additionally, the pore size distribution is consistent with the crystal structures, verifying the impact of the functional groups on pore size tuning (Fig. S23†).

Single-component adsorption and selectivity

Single-component adsorption isotherms of C_2H_2, C_2H_4 and C_2H_6 were collected for the three PCPs (Fig. 2b–d and S24–

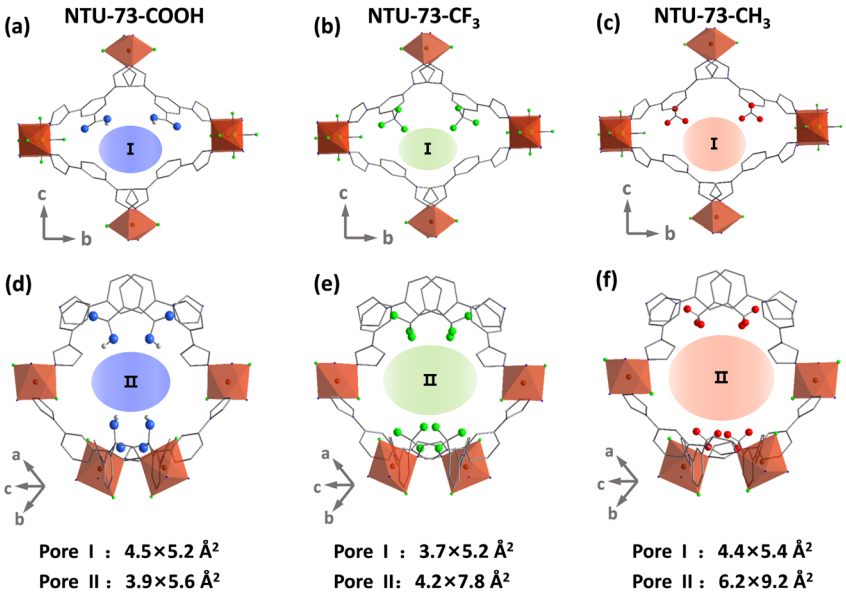

Fig. 1 Structure of the NTU-73-series: local views of the nanospace of NTU-73-COOH (a and d), NTU-73-CF_3 (b and e) and NTU-73-CH_3 (c and f) in different directions.

S35†), respectively. With the carboxylate pincers, exposed in the nanochannel, **NTU-73-COOH** shows the lowest gas uptake (C_2H_2: 32.3 $cm^3\ g^{-1}$, C_2H_4: 12.9 $cm^3\ g^{-1}$ and C_2H_6: 11.8 $cm^3\ g^{-1}$) among the three PCPs. Not only that, the adsorption capacity of C_2H_4 is slightly higher than that of C_2H_6, indicating an impossible harvesting of pure C_2H_4 in one-step from the ternary C2 mixtures, although it shows promising ability in binary C_2H_2/C_2H_4 separation. After replacing the –COOH groups with –CF_3 groups, **NTU-73-CF_3** shows a significantly increased gas uptake at 100 kPa (C_2H_2: 77.7 $cm^3\ g^{-1}$, C_2H_4: 62.0 $cm^3\ g^{-1}$, and C_2H_6: 62.7 $cm^3\ g^{-1}$), in which the C_2H_6 uptake is slightly higher than that of C_2H_4. Comparing the structural nature of the above two, the decrease in the polarity of the pore surface could alter the sequence of host–C_2H_4 and –C_2H_6 interactions. As expected, the adsorption capacities of C2 gases show a further increase in **NTU-73-CH_3** (C_2H_2: 98.0 $cm^3\ g^{-1}$; C_2H_4: 77.8 $cm^3\ g^{-1}$; C_2H_6: 89.9 $cm^3\ g^{-1}$), particularly, the C_2H_6 uptake is higher than that of C_2H_4 (12.1 $cm^3\ g^{-1}$, 100 kPa, 298 K). Notably, this uptake difference is much higher than that of the benchmark materials of MOF-303 (−0.5 $cm^3\ g^{-1}$),[41] NPU-1 (6.7 $cm^3\ g^{-1}$),[31] TJT-100 (5.8 $cm^3\ g^{-1}$),[11] and is approaching that of Al-PyDC (17.0 $cm^3\ g^{-1}$, 296 K)[33] and UPC-612 (17.5 $cm^3\ g^{-1}$)[6] (Table S3†). In addition,

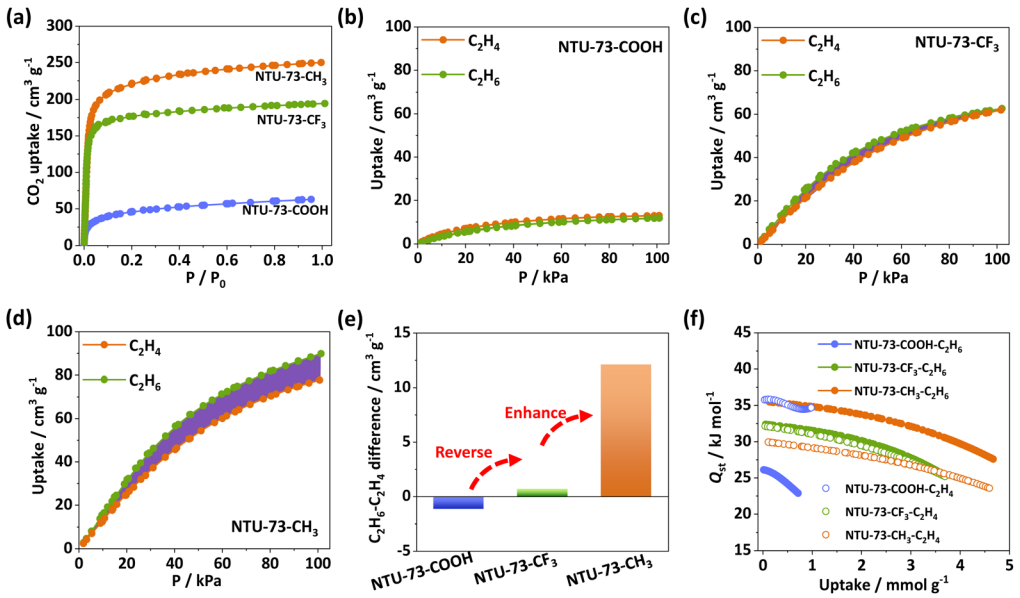

Fig. 2 CO_2-adsorption isotherms of the NTU-73-series at 195 K (a). C_2H_4 and C_2H_6 adsorption isotherms of NTU-73-COOH (b), NTU-73-CF_3 (c), and NTU-73-CH_3 (d) at 298 K. Uptake difference (e) and isosteric heats (f) of the three PCPs.

despite the gradual decrease in pore channel polarity, C_2H_2 uptake is always higher than that of C_2H_4, about 20.0 $cm^3\ g^{-1}$, in the **NTU-73-series** (Fig. 2e and S36†). In other words, systematically tuned organic sites endow significant functional changes, where **NTU-73-CH$_3$** is expected to achieve efficient C_2H_4 purification from C2 ternary mixtures.

Static adsorption selectivity and isosteric heats

To further evaluate the gas separation performance, the adsorption selectivities of C_2H_6/C_2H_4 and C_2H_2/C_2H_4 at 298 K were calculated *via* the ideal adsorbed solution theory (IAST) after fitting the single-component adsorption isotherms to the Langmuir–Freundlich equation (Fig. S37–S49†). For the equimolar C_2H_6/C_2H_4 mixtures, the adsorption selectivity values were found to be 0.66 for **NTU-73-COOH**, 1.18 for **NTU-73-CF$_3$** and 1.33 for **NTU-73-CH$_3$**. Importantly, the selectivity of **NTU-73-CH$_3$** is higher than that of TJT-100 (1.2) and NPU-1 (1.32), and close to that of UPC-612 (1.4), MOF-303 (1.7), Al-PyDC (1.9, 296 K) under almost the same conditions (Table S3†). Additionally, among the top-tier (C_2H_6–C_2H_4 uptake difference larger than 10 $cm^3\ g^{-1}$) C_2H_2–C_2H_6-selective adsorbents, the C_2H_2/C_2H_4 (1/99, v/v) selectivity (3.2 at 298 K, 100 kPa) of **NTU-73-CH$_3$** is only lower than that of Al-PyDC (4.3 at 296 K, 100 kPa) (Table S4†). Therefore, the high C_2H_6–C_2H_4 uptake difference and the good selectivities make **NTU-73-CH$_3$** a promising candidate for C_2H_4 purification from C2 ternary mixtures.

To evaluate the interaction strength of C_2H_2, C_2H_4 and C_2H_6 in the **NTU-73-series**, the isosteric heat (Q_{st}) was calculated after fitting the adsorption isotherms by the virial equation at 273, 283 and 298 K, respectively (Fig. 2f and S50–S59†). The Q_{st} value of C_2H_2 (**NTU-73-COOH**: 41.00 kJ mol^{-1}, **NTU-73-CF$_3$**: 39.83 kJ mol^{-1}, **NTU-73-CH$_3$**: 37.06 kJ mol^{-1}) is higher than that of C_2H_4 (**NTU-73-COOH**: 35.78 kJ mol^{-1}, **NTU-73-CF$_3$**: 32.12 kJ mol^{-1}, **NTU-73-CH$_3$**: 29.90 kJ mol^{-1}) and C_2H_6 (**NTU-73-COOH**: 26.10 kJ mol^{-1}, **NTU-73-CF$_3$**: 32.39 kJ mol^{-1}, **NTU-73-CH$_3$**: 35.43 kJ mol^{-1}) in the **NTU-73-series** at low coverage, while an inversion of the host–C_2H_4 and host–C_2H_6 interactions was observed: a higher Q_{st} of C_2H_4 over C_2H_6 in **NTU-73-COOH** changes to a higher Q_{st} of C_2H_6 over C_2H_4 in **NTU-73-CH$_3$**. These observations are consistent with the adsorption isotherms. In addition, these relatively low adsorption enthalpy values indicate a relatively low energy consumption for regeneration of the PCPs.

Gas-loaded crystallographic and Raman analysis

The isosteric heat is a kind of statistical result, making it difficult to accurately describe the role of functional sites. Therefore, to better explore the reversal phenomenon of C_2H_4 and C_2H_6 adsorption and Q_{st} values, gas-loaded crystallographic analysis was performed at 298 K (Fig. 3 and Table S5†).[42] Despite the disordered nature, the trapped gases can be clearly found in these three PCPs. For **NTU-73-COOH⊃C$_2$H$_4$**, two C_2H_4 molecules form three hydrogen bonds with the $\mathbf{O_{COOH}}$ of the free carboxylic pincers, of which, the shortest distance is 1.8973 Å. Meanwhile, intermolecular interactions ($dC_{C_2H_4}$–H$\cdots$$C_{C_2H_4}$: 2.3748 to 2.8025 Å) have been found between these two molecules (Fig. 3a). For **NTU-73-COOH⊃C$_2$H$_6$**, two groups of hydrogen bonds ($dC_{C_2H_6}$–H$\cdots$$O_{COOH}$: 2.3338 to 2.9779 Å and g $C_{C_2H_6}$–H$\cdots$$N_{imidazole}$) with relatively longer distances were observed. In addition, the slightly larger distance leads to the disappearance of the intermolecular interactions (Fig. 3b). This clear change can therefore explain the fact that **NTU-73-COOH** binds C_2H_4 more strongly than C_2H_6. However, in contrast to our expectation, the distance between the gases and the –CF_3 group is relatively far. So as that, both molecules are located around the coordinated ZrF_6^{2-} ions. This is due to the relatively weak degree of electronegativity of F_{CF_3} compared to that of F_{ZrF_6}. However, the presence of the –CF_3 group influences the configuration of the adsorbed gas molecules. As can be seen, the two F atoms of ZrF_6^{2-} form two hydrogen bonds with C_2H_4 and C_2H_6, respectively. The shortest distances of the hydrogen bonds ($dC_{C_2H_6}$–H$\cdots$$F_{ZrF_6}$: 2.6094 Å and $dC_{C_2H_4}$–H$\cdots$$F_{ZrF_6}$: 2.6647

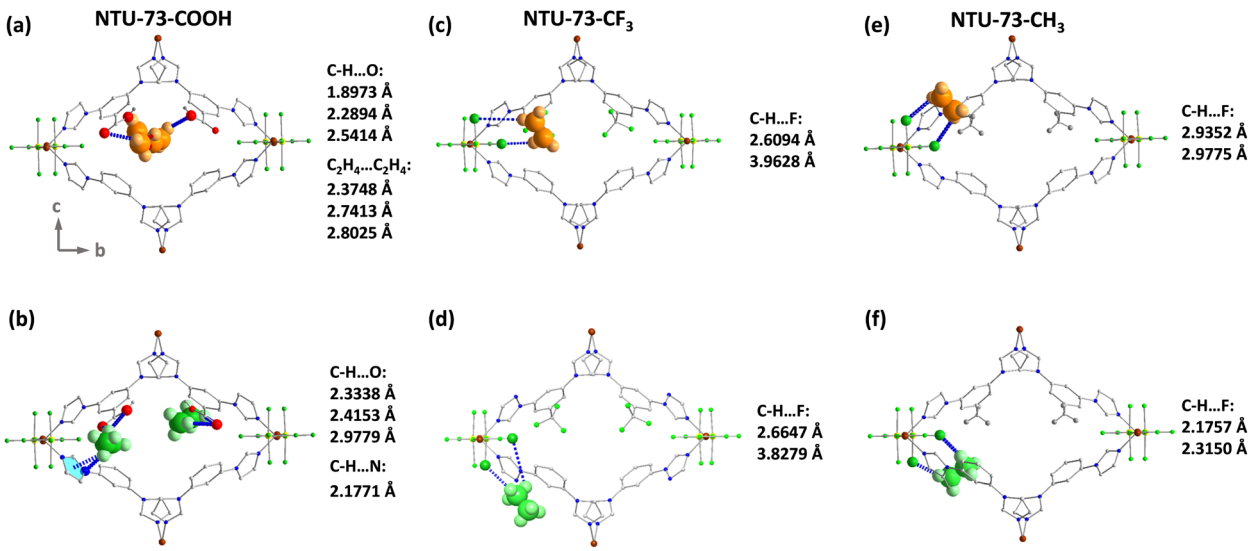

Fig. 3 C_2H_4- and C_2H_6-loaded crystallographic analysis of NTU-73-COOH (a and b), NTU-73-CF_3 (c and d) and NTU-73-CH_3 (e and f).

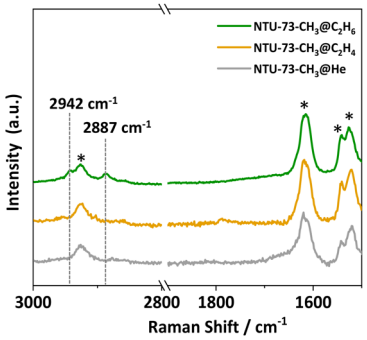

Fig. 4 Raman spectra of gas-loaded **NTU-73-CH$_3$** (the peaks marked with * derived from the framework).

Å) are very close to each other, indicating similar host–guest interactions (Fig. 3c and d). In **NTU-73-CH$_3$**, both gases are also observed around the coordinated ZrF_6^{2-} ions. Without the withdrawal effect of the organic F sites from $-CF_3$, the configuration of the adsorbed C_2H_4 shows a slight change, wherein the distance of the two hydrogen bonds ($C_{C_2H_4}$–H···F_{ZrF_6}) becomes close to each other (2.9352 Å and 2.9775 Å) (Fig. 3e). Additionally, the end-on mode of $C_{C_2H_6}$–H···F_{ZrF_6} in **NTU-73-CF$_3$** changes to a chelate connection in **NTU-73-CH$_3$**; particularly, the distance of the two $C_{C_2H_6}$–H···F_{ZrF_6} (2.1757 Å and 2.3150 Å) is shorter than that of $C_{C_2H_4}$–H···F_{ZrF_6} in **NTU-73-CF$_3$** (Fig. 3f). Therefore, these results not only explain the phenomenon of the adsorption trend of C_2H_4 and C_2H_6 in **NTU-73-series**, but also can strengthen the molecular insights of fine-tuning the pore environment by functional organic groups.

Given the promising nature of **NTU-73-CH$_3$**, the stabilizing effect of the pore environment towards C_2H_4 and C_2H_6 was further evaluated by Raman spectra. After dosing a highly pure gas (He, C_2H_4 or C_2H_6, 1 bar, 298 K) into the glass tube with fully activated **NTU-73-CH$_3$**, respectively, the corresponding spectra were recorded in the range of 1000 to 4000 cm^{-1} (Fig. 4 and S60†). As can be seen, the peaks at 2887 cm^{-1} and 2942 cm^{-1} belonging to the stretching vibration of C_2H_6 have been identified,[43] but no additional peaks other than those belonging to **NTU-73-CH$_3$** were observed under the C_2H_4 atmosphere (theoretical position: 1689 cm^{-1}). Therefore, it is clear that **NTU-73-CH$_3$** not only has a relatively stronger host–C_2H_6 interaction, but also can stabilize a certain number of C_2H_6 molecules in a periodic arrangement, which is consistent with the results of the crystallographic analysis.

Breakthrough experiments

To validate the separation performance under dynamic conditions, breakthrough experiments were conducted on the **NTU-73-series** (Fig. 5 and S61–S69†). All initially activated samples were loaded into the column and further activation was achieved by He sweeping until no signals were detected. Breakthrough experiments were then carried out using a binary mixture of C_2H_2/C_2H_4 (1 : 99, v/v) at first, a typical industrial composition. Compared to **NTU-73-COOH**, both **NTU-73-CF$_3$** and **NTU-73-CH$_3$** showed a certain loss of breakthrough time interval, but still demonstrated the separation ability towards C_2H_2/C_2H_4. Further experiments were conducted on C_2H_6/C_2H_4 mixtures. At a volume ratio of 1 : 15, C_2H_6 breaks through slightly earlier than C_2H_4 for the **NTU-73-COOH** sample bed. Interestingly, high purity C_2H_4 can be obtained directly at the outlet of the **NTU-73-CF$_3$** and **NTU-73-CH$_3$** columns, of which, **NTU-73-CH$_3$** has a longer C_2H_6–C_2H_4 breakthrough interval than **NTU-73-CF$_3$** (4.8 min g^{-1} *vs.* 4.0 min g^{-1}). To further

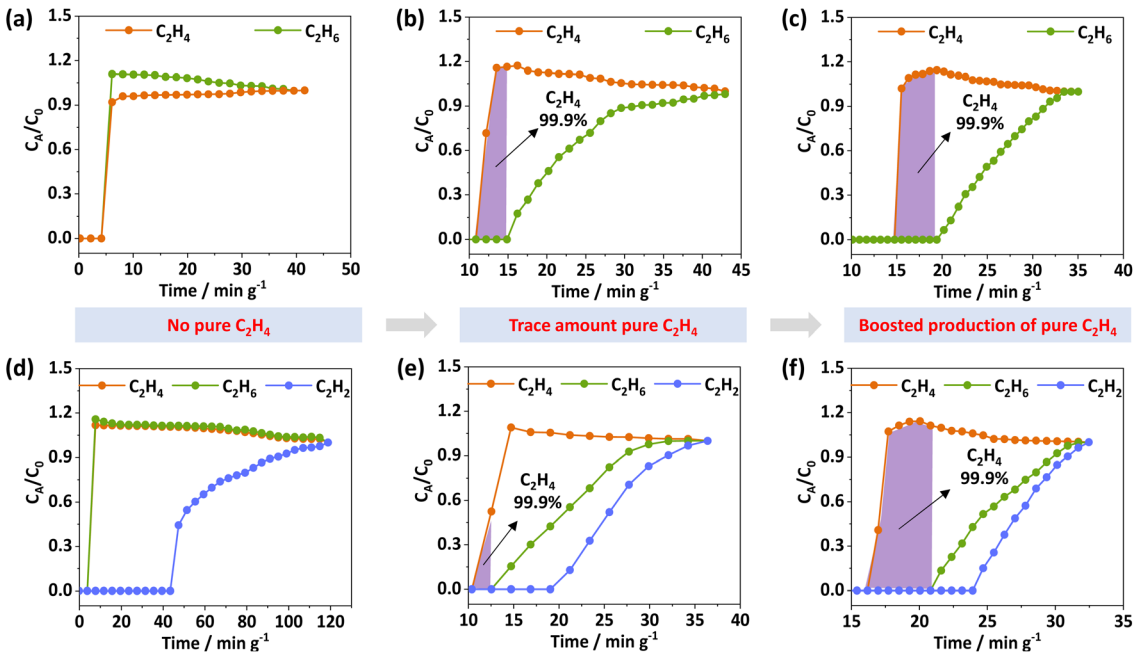

Fig. 5 Experimental breakthrough curves of **NTU-73-COOH** (a and d), **NTU-73-CF$_3$** (b and e), and **NTU-73-CH$_3$** (c and f) for C_2H_6/C_2H_4 (1/9, v/v, 2 mL min^{-1}) and $C_2H_2/C_2H_6/C_2H_4$ (1/9/90, v/v/v, 2 mL min^{-1}) mixtures, respectively at 298 K. The gas pressure is 1.4 bar for all experiments.

investigate the influence of ratio on this separation, a feed gas with a ratio of 1 : 9, the most common ratio found in the cracking process, was introduced into the column. **NTU-73-COOH** was unable to separate this mixture, while **NTU-73-CF_3** and **NTU-73-CH_3** retained their separation abilities. Among them, **NTU-73-CH_3** showed the longest breakthrough time interval (4.6 min g^{-1} *vs.* 2.7 min g^{-1} *vs.* 0 min g^{-1}), owing to its higher selectivity for C_2H_6/C_2H_4 and its greater uptake capacity for C_2H_6 (Fig. 5a–c). This trend was also observed in experiments using equimolar C_2H_6/C_2H_4 mixtures.

Encouraged by the successful separation of the binary mixtures, C_2H_2/C_2H_4 and C_2H_6/C_2H_4, the separation ability of the NTU-73-series towards ternary mixtures $C_2H_2/C_2H_6/C_2H_4$ (1/9/90, v/v/v) was further investigated, respectively. As expected, both C_2H_6 and C_2H_4 elute out simultaneously from the **NTU-73-COOH** bed (Fig. 5d). Despite the separation potential, high-yield C_2H_4 cannot be produced by **NTU-73-CF_3** (Fig. 5e). Only **NTU-73-CH_3** allows significant production of high purity (>99.9%) C_2H_4 (0.52 mmol g^{-1} (STP)) (Fig. 5f and S70†). This value is higher than that of CAU-23 (0.18 mmol g^{-1}), TJT-100 (0.41 mmol g^{-1}), and UPC-612 (0.47 mmol g^{-1}), but lower than that of MOF-303 (1.35 mmol g^{-1}) and Azole-Th-1 (1.34 mmol g^{-1}) (Tables S3 and S4†).

Stability and recyclability

Stability is another crucial factor in measuring the performance of adsorbents.[44] The crystals of **NTU-73-COOH**, **NTU-73-CF_3** and **NTU-73-CH_3** were immersed in chemical solutions (pH = 2, pH = 7 and pH = 12) for 3 days or exposed to air for 7 days, respectively. The PXRD patterns of the samples were then collected and compared with the simulated patterns (Fig. S71–S73†). The results reveal that some of the characteristic peaks of **NTU-73-COOH** and **NTU-73-CF_3** were weakened or disappeared after immersion in certain solutions, in particular, the diffraction peaks almost completely disappeared in the alkaline solution (pH = 12), suggesting the structural instability. However, the crystals of **NTU-73-CH_3** retained almost the same diffraction peaks after treatment under these harsh conditions. Additionally, the C_2H_6 uptakes of these treated samples are nearly the same (Fig. S74†), indicating that the introduction of the hydrophobic $-CH_3$ group plays a crucial role in protecting the coordination bonds and then stabilizing the framework. Thanks to this good stability, **NTU-73-CH_3** demonstrates no loss of performance during the cycling breakthrough experiments (Fig. S75†).

Conclusions

In response to the demand for C_2H_4 purification, we herein report an approach of systematic tuning of the porous environment with organic sites (from –COOH to $-CF_3$ and then to $-CH_3$) in PCPs, wherein the highly stable **NTU-73-CH_3** exhibits remarkable capability for direct production of poly-grade C_2H_4 from ternary C2 hydrocarbons under ambient conditions. In addition, the molecular insights derived from *in situ* crystallographic and Raman analysis confirm the positive effect of the $-CH_3$ group in tuning the configuration and strength of the adsorbed C_2H_4 and C_2H_6. This study not only highlights the importance of systemic regulation, but also illustrates how changes in functional groups within PCPs can profoundly affect the host–guest interaction and separation performance. Moreover, the strategy of systematic organic functionalization can be extended to other porous families, offering a powerful tool for tailoring high-performance PCPs for desired applications.

Data availability

All data can be found in the main text and ESI.†

Author contributions

J. D. and W. J. conceived the idea of this work. Y. L. carried out the experiments and analyzed the results. J. D. and Y. L. wrote the paper. All authors gave valuable suggestions for the final draft.

Conflicts of interest

The authors declare no competing interests.

Acknowledgements

We are thankful for the financial support of the National Natural Science Foundation of China (22171135), the National Natural Science Foundation of Jiangsu Province (BK20231269) and the State Key Laboratory of Materials-Oriented Chemical Engineering (SKL-MCE-23A18).

References

1 S. Gong, C. Shao and L. Zhu, *Energy*, 2021, **217**, 119401.
2 S. M. Sadrameli, *Fuel*, 2016, **173**, 285–297.
3 G. D. Wang, Y. Z. Li, W. J. Shi, L. Hou, Y. Y. Wang and Z. Zhu, *Angew. Chem., Int. Ed.*, 2022, **61**, e202205427.
4 Z. B. Bao, D. Y. Xie, G. G. Chang, H. Wu, L. Y. Li, W. Zhou, H. L. Wang, Z. G. Zhang, H. B. Xing, Q. W. Yang, M. J. Zaworotko, Q. L. Ren and B. L. Chen, *J. Am. Chem. Soc.*, 2018, **140**, 4596–4603.
5 Q. Ding, Z. Zhang, Y. Liu, K. Chai, R. Krishna and S. Zhang, *Angew. Chem., Int. Ed.*, 2022, **61**, e202208134.
6 Y. T. Wang, C. L. Hao, W. D. Fan, M. Y. Fu, X. K. Wang, Z. K. Wang, L. Zhu, Y. Li, X. Q. Lu, F. N. Dai, Z. X. Kang, R. M. Wang, W. Y. Guo, S. Q. Hu and D. F. Sun, *Angew. Chem., Int. Ed.*, 2021, **60**, 11350–11358.
7 F. Studt, F. Abild-Pedersen, T. Bligaard, R. Z. Sorensen, C. H. Christensen and J. K. Norskov, *Science*, 2008, **320**, 1320–1322.
8 Z. Xu, X. Xiong, J. Xiong, R. Krishna, L. Li, Y. Fan, F. Luo and B. Chen, *Nat. Commun.*, 2020, **11**, 3163–3172.
9 K. Z. Su, W. J. Wang, S. F. Du, C. Q. Ji and D. Q. Yuan, *Nat. Commun.*, 2021, **12**, 3703–3710.
10 J.-W. Cao, S. Mukherjee, T. Pham, Y. Wang, T. Wang, T. Zhang, X. Jiang, H.-J. Tang, K. A. Forrest, B. Space,

M. J. Zaworotko and K.-J. Chen, *Nat. Commun.*, 2021, **12**, 6507–6515.
11 H. G. Hao, Y. F. Zhao, D. M. Chen, J. M. Yu, K. Tan, S. Q. Ma, Y. Chabal, Z. M. Zhang, J. M. Dou, Z. H. Xiao, G. Day, H. C. Zhou and T. B. Lu, *Angew. Chem., Int. Ed.*, 2018, **57**, 16067–16071.
12 Z. Q. Zhang, S. B. Peh, Y. X. Wang, C. J. Kang, W. D. Fan and D. Zhao, *Angew. Chem., Int. Ed.*, 2020, **59**, 18927–18932.
13 S. H. Yang, A. J. Ramirez-Cuesta, R. Newby, V. Garcia-Sakai, P. Manuel, S. K. Callear, S. I. Campbell, C. C. Tang and M. Schroder, *Nat. Chem.*, 2015, **7**, 121–129.
14 P. Q. Liao, W. X. Zhang, J. P. Zhang and X. M. Chen, *Nat. Commun.*, 2015, **6**, 8697–8706.
15 C. Gu, N. Hosono, J. J. Zheng, Y. Sato, S. Kusaka, S. Sakaki and S. Kitagawa, *Science*, 2019, **363**, 387–391.
16 Q. Ding, Z. Q. Zhang, C. Yu, P. X. Zhang, J. Wang, X. L. Cui, C. H. He, S. G. Deng and H. B. Xing, *Sci. Adv.*, 2020, **6**, 122617.
17 C. H. He, Y. Wang, Y. Chen, X. Q. Wang, J. F. Yang, L. B. Li and J. P. Li, *ACS Appl. Mater. Interfaces*, 2020, **12**, 52819–52825.
18 L. C. Jiang, Y. Y. Tian, T. Sun, Y. L. Zhu, H. Ren, X. Q. Zou, Y. H. Ma, K. R. Meihaus, J. R. Long and G. S. Zhu, *J. Am. Chem. Soc.*, 2018, **140**, 15724–15730.
19 Y. Z. Liu, Y. Wu, W. W. Liang, J. J. Peng, Z. Li, H. H. Wang, M. J. Janik and J. Xiao, *Chem. Eng. Sci.*, 2020, **220**, 115636.
20 P. J. Bereciartua, A. Cantin, A. Corma, J. L. Jorda, M. Palomino, F. Rey, S. Valencia, E. W. Corcoran, P. Kortunov, P. I. Ravikovitch, A. Burton, C. Yoon, Y. Wang, C. Paur, J. Guzman, A. R. Bishop and G. L. Casty, *Science*, 2017, **358**, 1068–1071.
21 Y. C. Chai, X. Han, W. Y. Li, S. S. Liu, S. K. Yao, C. Wang, W. Shi, I. Da-Silva, P. Manuel, Y. Q. Cheng, L. D. Daemen, A. J. Ramirez-Cuesta, C. C. Tang, L. Jiang, S. H. Yang, N. J. Guan and L. D. Li, *Science*, 2020, **368**, 1002–1006.
22 W. W. Liang, Y. Wu, H. Y. Xiao, J. Xiao, Y. W. Li and Z. Li, *Chem.–Eur. J.*, 2018, **64**, 3390–3399.
23 C. Xiao, J. D. Tian, Q. H. Chen and M. C. Hong, *Chem. Sci.*, 2024, **15**, 1570–1610.
24 P. Zhang, Y. Zhong, Y. Zhang, Z. Zhu, Y. Liu, Y. Su, J. Chen, S. Chen, Z. Zeng, H. Xing, S. Deng and J. Wang, *Sci. Adv.*, 2022, **8**, eabn9231.
25 K. J. Chen, D. G. Madden, S. Mukherjee, T. Pham, K. A. Forrest, A. Kumar, B. Space, J. Kong, Q. Y. Zhang and M. J. Zaworotko, *Science*, 2019, **366**, 241–246.
26 Q. Ding, Z. Q. Zhang, Y. L. Liu, K. G. Chai, R. Krishna and S. Zhang, *Angew. Chem., Int. Ed.*, 2022, **61**, e202208134.
27 M. Kang, S. Yoon, S. Ga, D. W. Kang, S. Han, J. H. Choe, H. Kim, D. W. Kim, Y. G. Chung and C. S. Hong, *Adv. Sci.*, 2021, **8**, 2004940.
28 M. J. Kang, D. W. Kang, J. H. Choe, H. Kim, D. W. Kim, H. Park and C. S. Hong, *Chem. Mater.*, 2021, **33**, 6193–6199.
29 J. Y. Pei, J. X. Wang, K. Shao, Y. Yang, Y. J. Cui, H. Wu, W. Zhou, B. Li and G. D. Qian, *J. Mater. Chem. A*, 2020, **8**, 3613–3620.
30 R. B. Lin, H. Wu, L. B. Li, X. L. Tang, Z. Q. Li, J. K. Gao, H. Cui, W. Zhou and B. L. Chen, *J. Am. Chem. Soc.*, 2018, **140**, 12940–12946.
31 B. Y. Zhu, J. W. Cao, S. Mukherjee, T. Pham, T. Zhang, T. Wang, X. Jiang, K. A. Forrest, M. J. Zaworotko and K. J. Chen, *J. Am. Chem. Soc.*, 2021, **143**, 1485–1492.
32 X. W. Gu, J. X. Wang, E. Y. Wu, H. Wu, W. Zhou, G. D. Qian, B. L. Chen and B. Li, *J. Am. Chem. Soc.*, 2022, **144**, 2614–2623.
33 E. Wu, X.-W. Gu, D. Liu, X. Zhang, H. Wu, W. Zhou and G. Qian, *Nat. Commun.*, 2023, **14**, 6146–6157.
34 H. R. Sun, F. Q. Chen, R. D. Chen, J. Q. Li, L. D. Guo, Y. Liu, F. X. Shen, Q. W. Yang, Z. G. Zhang, Q. L. Ren and Z. B. Bao, *Small*, 2023, **19**, 2208182.
35 Q. Dong, X. Zhang, S. Liu, R. B. Lin, Y. Guo, Y. Ma, A. Yonezu, R. Krishna, G. Liu, J. Duan, R. Matsuda, W. Jin and B. Chen, *Angew. Chem., Int. Ed.*, 2020, **59**, 22756–22762.
36 Q. Dong, Y. Huang, K. Hyeon-Deuk, I. Y. Chang, J. Wan, C. Chen, J. Duan, W. Jin and S. Kitagawa, *Adv. Funct. Mater.*, 2022, **32**, 2203745.
37 Y. Huang, J. Wan, T. Pan, K. Ge, Y. Guo, J. Duan, J. Bai, W. Jin and S. Kitagawa, *J. Am. Chem. Soc.*, 2023, **145**, 24425–24432.
38 J. Wan, H. L. Zhou, K. Hyeon-Deuk, I. Y. Chang, Y. Huang, R. Krishna and J. Duan, *Angew. Chem., Int. Ed.*, 2023, **62**, e202316792.
39 H. Wang, Y. Duan, Y. Wang, Y. Huang, K. Ge, S. Wang, B. Zheng, Z. Wang, J. Bai and J. Duan, *ACS Appl. Mater. Interfaces*, 2022, **14**, 13550–13559.
40 Y. F. Duan, Y. H. Huang, C. Q. Wang, Q. Wang, K. Ge, Z. Y. Lu, H. J. Wang, J. G. Duan, J. F. Bai and W. Q. Jin, *Chem. Sci.*, 2023, **14**, 4605–4611.
41 H.-M. Wen, C. Yu, M. Liu, C. Lin, B. Zhao, H. Wu, W. Zhou, B. Chen and J. Hu, *Angew. Chem., Int. Ed.*, 2023, **62**, e202309108.
42 Q. Dong, Y. Huang, J. Wan, Z. Lu, Z. Wang, C. Gu, J. Duan and J. Bai, *J. Am. Chem. Soc.*, 2023, **145**, 8043–8051.
43 R. Fantoni, K. Vanhelvoort, W. Knippers and J. Reuss, *Chem. Phys.*, 1986, **110**, 1–16.
44 Q. B. Dong, J. M. Wan, H. H. Chen, Y. H. Huang and J. G. Duan, *ACS Appl. Mater. Interfaces*, 2023, **15**, 39606–39613.